Available online at www.sciencedirect.com

ScienceDirect

www.elsevier.com/locate/jmbbm

Research Paper

Compensation strategy to reduce geometry and mechanics mismatches in porous biomaterials built with Selective Laser Melting

*Zahra S. Bagheri, David Melancon, Lu Liu, R. Burnett Johnston, Damiano Pasini**

Department of Mechanical Engineering, McGill University, Montreal, QC, Canada H3G 1A4

ARTICLE INFO

Article history:
Received 2 March 2016
Received in revised form
21 April 2016
Accepted 27 April 2016
Available online 6 May 2016

Keywords:
Additive Manufacturing
Metallic porous biomaterials
Geometry mismatch
Mechanical properties
Compensation strategy

ABSTRACT

The accuracy of Additive Manufacturing processes in fabricating porous biomaterials is currently limited by their capacity to render pore morphology that precisely matches its design. In a porous biomaterial, a geometric mismatch can result in pore occlusion and strut thinning, drawbacks that can inherently compromise bone ingrowth and severely impact mechanical performance. This paper focuses on Selective Laser Melting of porous microarchitecture and proposes a compensation scheme that reduces the morphology mismatch between as-designed and as-manufactured geometry, in particular that of the pore. A spider web analog is introduced, built out of Ti–6Al–4V powder via SLM, and morphologically characterized. Results from error analysis of strut thickness are used to generate thickness compensation relations expressed as a function of the angle each strut formed with the build plane. The scheme is applied to fabricate a set of three-dimensional porous biomaterials, which are morphologically and mechanically characterized via micro Computed Tomography, mechanically tested and numerically analyzed. For strut thickness, the results show the largest mismatch (60% from the design) occurring for horizontal members, reduces to 3.1% upon application of the compensation. Similar improvement is observed also for the mechanical properties, a factor that further corroborates the merit of the design-oriented scheme here introduced.

1. Introduction

Additive processes provide an exciting opportunity to build metals with customized porous architecture and mechanical properties unachievable in monolithic materials (Ashby and Bréchet, 2003; Fleck et al., 2010; Schaedler et al., 2011). Porous biomaterials with tailored cell morphology enable cell proliferation and differentiation, required for bone ingrowth, as well as nutrient, oxygen and waste diffusion (Hutmacher, 2000; Yang et al., 2001; Sanz-Herrera et al., 2008). Furthermore, their

*Correspondence to: Department of Mechanical Engineering, McGill University, Macdonald Engineering Building, Rm 372 817 Sherbrooke West, Montreal, Quebec, Canada H3A 0C3. Tel.: +1 514 3986295.
E-mail address: damiano.pasini@mcgill.ca (D. Pasini).

http://dx.doi.org/10.1016/j.jmbbm.2016.04.041
1751-6161/

mechanical properties can be tuned to provide adequate strength and matched stiffness with respect to anatomical location (Hutmacher, 2000; Yang et al., 2001; Sanz-Herrera et al., 2008; Arabnejad Khanoki and Pasini, 2012, 2013a, 2013b). The functionality and overall success of porous biomaterials and implants depend upon a multitude of factors including pore morphology and interconnectivity, as well as their ability to fill bone defects (Hollister and Murphy, 2011; Wu et al., 2014). Conventional manufacturing methods for open-cell porous materials, such as solid state processing (sintering of fibers and powder metallurgy), liquid state processing (spray foaming, direct foaming), vapor deposition, and electro-deposition, often fail to produce porous implants with desired porosity and homogenous distribution of pores for sufficient bone ingrowth (Ryan et al., 2006; Banhart, 2001). As an alternative, Additive Manufacturing (AM) processes, such as Electron Beam Melting (EBM) and Selective Laser Melting (SLM), are layer-by-layer technology enabling custom porous implants with internal architecture (Murr et al., 2010; Van Bael et al., 2011; Williams et al., 2005; Pattanayak et al., 2011; Heinl et al., 2008; Parthasarathy et al., 2010) and mechanical response tuned to those of the surrounding bone tissue, and pore morphology tailored to ease bone ingrowth (Sobral et al., 2011; Khoda et al., 2010).

Although AM allows control of pore architecture, current technologies fail short in reproducing cellular geometry at the expected level of fidelity and accuracy. Geometry discrepancies often appear between the as-designed and as-manufactured pore geometry, especially for architecture with element size reaching the manufacturing limits (Parthasarathy et al., 2010; Arabnejad et al., 2016a; Yan et al., 2012). The problem is serious not only because a geometry mismatch can result in pore occlusion, which in turn impair osseointegration, but also because the resulting mechanical properties can be far off from the expected values (Parthasarathy et al., 2010; Arabnejad et al., 2016a; Yan et al., 2012; Hollander et al., 2006; Mullen et al., 2010).

Previous studies have shown that strut thickness, strut cross section, strut straightness, and pore size are among the variables that most suffer from AM inaccuracy (Parthasarathy et al., 2010; Arabnejad et al., 2016a; Yan et al., 2012; Hollander et al., 2006; Mullen et al., 2010). In particular, strut thickness has been shown to be highly dependent on the angle a strut forms with the build plane. Well documented in the literature, this deviation is attributed to a difference in heat transfer properties between solid struts and their surrounding powder. For example, Gebhardt et al. (2014) reported severe stair-climbing effect for struts at 45° angle from the build plane with noticeable amount of adherent particles for struts at 90°. Several methods have been proposed to reduce the error inherent to the manufacturing process. They can be categorized in either design-oriented (Dias et al., 2014), or process-control strategies, which involve machine parameter tuning (Eshraghi and Das, 2010; Partee et al., 2005) and post-processing, such as electro polishing and acid etching (Pyka et al., 2012).

This paper introduces a design scheme to reduce fabrication deviations appearing in Ti–6Al–4V porous biomaterials built with SLM. A statistically meaningful set of spider-webs were designed with struts built at varying build angles, built with prescribed in-plane strut thickness, which in turn were measured via light microscopy. Exponential interpolation functions of the relative error appearing from the designed thickness were correlated to the build plane angle. These relations are at the core of compensation relations that enable the generation of compensated geometries that are built with higher accuracy. The scheme was experimentally validated on a spider web analog, and then applied to a set of three-dimensional porous biomaterials. Micro-CT morphological characterization, as well as mechanical property analysis conducted on compensated and uncompensated geometries, demonstrated the merit of the procedure here introduced.

2. Compensation strategy

Additive processes of metallic lattices often result in fabricated pores which contain deviations from their as-designed geometry. Fig. 1 illustrates the unit cell of a typical lattice built with SLM, where the comparison of *as-manufactured* and *as-designed* geometry points out several morphological mismatches, including formation of parasitic mass at the joints, staircase effect of diagonal struts and strut thickness heterogeneity. With respect to the latter, the figure shows that

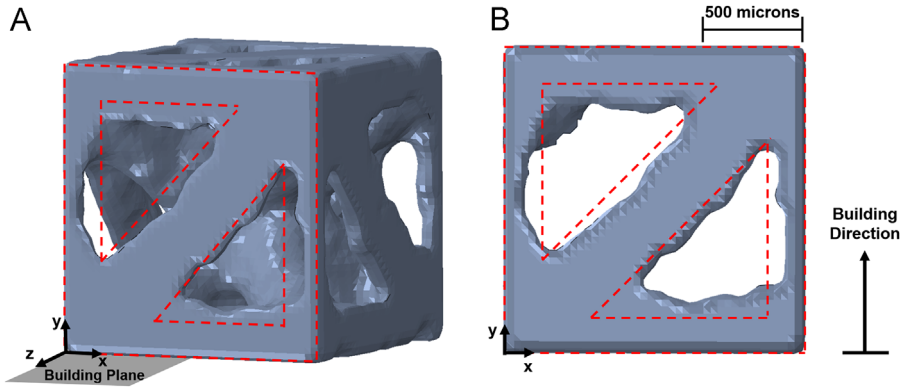

Fig. 1 – Three-dimensional reconstructed geometry of a SLM manufactured tetrahedron-based unit cell. A. Isometric view. B. Front view. Hidden lines (red) specify the ideal as-designed geometry of the unit cell. (For interpretation of the references to color in this figure legend, the reader is referred to the web version of this article.)

struts horizontally built with respect to the build plane are clearly overmelted and thicker than expected (red). Struts at increasing build angle, on the other hand, show decreased overmelting, which for vertical struts even results in under-sized thickness.

To reduce the mismatch between as-designed and as-produced geometry, we focus in this work on one, among others, important factor, i.e. the orientation angle formed by a strut with respect to the build plane (Van Bael et al., 2011; Arabnejad et al., 2016a; Yan et al., 2014). The approach that we take here is designed-oriented, rather than process control, in the sense that for given process parameters, our goal is first to predict and compensate strut thickness deviations expressed as a function of the angle with the build plane, and then generate a compensated geometry to manufacture. The scheme we propose here, uses a planar sample, a spider-web (Fig. 2A.), with struts oriented at given build plane angles. As shown in Fig. 2, it consists of a sturdy assessment of strut thickness deviations obtained with strut morphology characterization, error analysis, definition of compensation factors, and generation of spider-web geometry with compensated strut thickness. The model driving geometry compensation penalizes over-sized struts and augments those that are under-sized with correction factors dependent

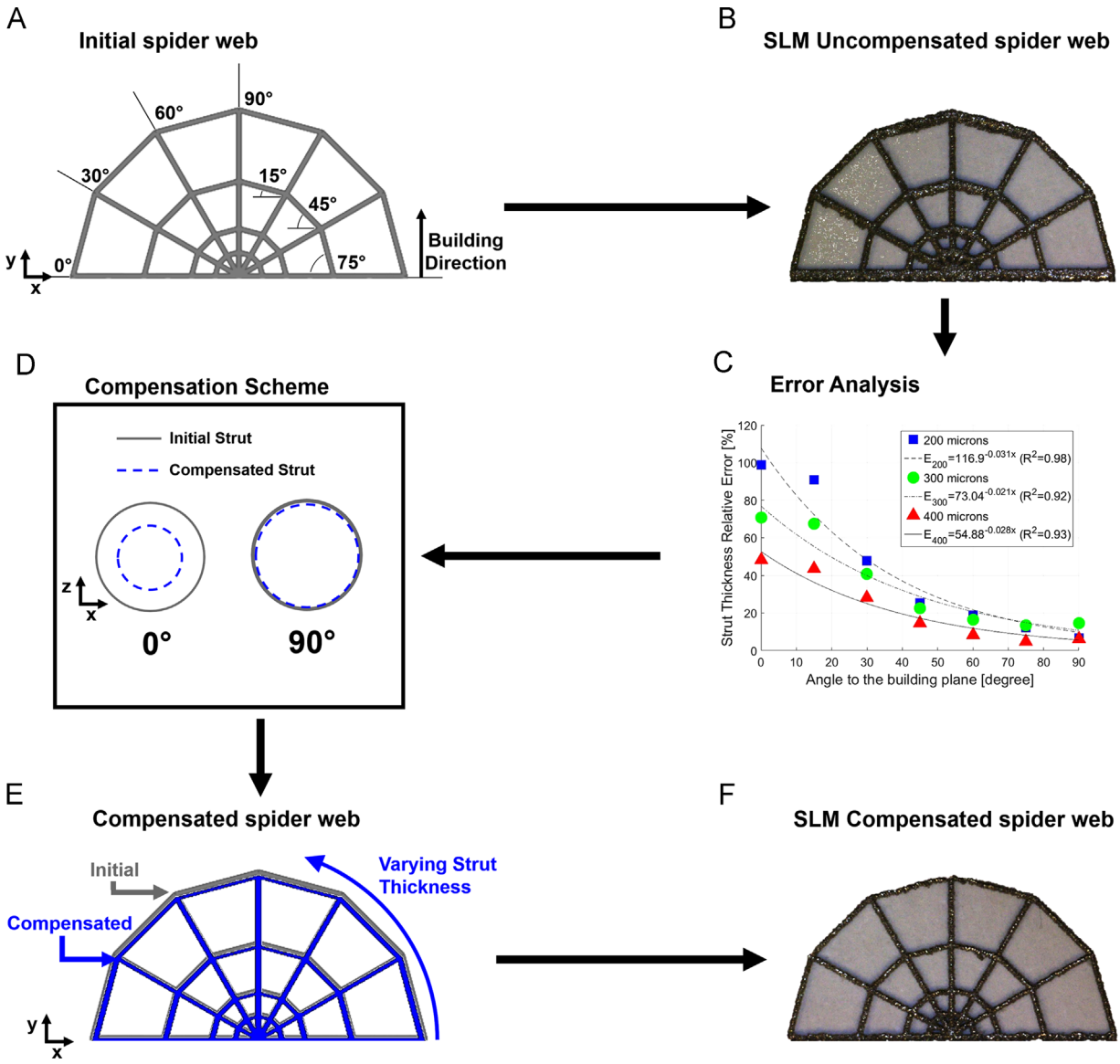

Fig. 2 – Design strategy scheme. A. Initial spider-web geometry with uniform strut thickness. B. SLM manufacturing of initial spider-web showing heterogeneous distribution of strut thickness. C. Analysis of strut thickness errors, each with respect to its design value, and expressed as a function of the angle with the build plane (*x*-axis) and the strut thickness (*E*: relative error for design strut thickness of 200, 300, and 400 μm; and R^2 correlation coefficient). D. Development and application of error compensation relations (described in Section 2.2). E. Generation of final spider-web geometry with varying strut thickness; the original spider-web design (gray) is superimposed the compensated one (blue). F. Manufacturing of compensated spider-web with geometry resembling the initial one (A) with uniform strut thickness. (For interpretation of the references to color in this figure legend, the reader is referred to the web version of this article.)

on the strut angle. As a result, the final strut thickness reaches the original target after the intrinsic overmelting induced by the manufacturing process. We chose a planar geometry for the spider-web, since it can be rapidly examined via light microscopy, as described in detail in the following section. In addition, it is effective in evaluating strut thickness deviations in three-dimensional lattices, as described in Section 3.

2.1. Design and fabrication of a multi-angle strut model, the spider-web

Fig. 2A. shows the spider-web geometry, with circular cross section struts at build angles varying from 0° to 90° at 15° increments. The spider-web were designed using SolidWorks (Dassault Systèmes SolidWorks Corporation, Waltham, MA). To investigate the dependency of strut in-plane thickness, three samples with uniform thickness of 200, 300, and 400 μm were built. These values lie in the relevant range and design constraints for porous metallic biomaterials (Arabnejad et al., 2016a). Its out-of-plane thickness is generally not influenced by the build angle and here set equal to the corresponding in-plane thickness. For each strut thickness, five spider-web replicates were fabricated via SLM out of Ti–6Al–4V powder (Renishaw AM-250, England). The manufacturing process was conducted on a titanium base plate in a closed chamber flushed with argon gas to reduce the level of interstitial elements, such as nitrogen, carbon, hydrogen and oxygen, and their subsequent reactivity with Ti–6Al–4V powder. A 100 W laser was chosen with a spot diameter of 70 μm. The samples were fabricated with a laser beam compensation of 50 μm. The point distance was 75 μm, exposure time was 60 ms and hatch spacing was 75 μm. Samples were removed from the build plate using Electrical Discharge Machining (EDM), and imaged via two-dimensional light microscopy to measure with ImageJ software (National Institute of Health, USA) strut thickness across all the angles (Rasband, 1997–2015).

2.2. Generation of thickness compensation relations

Fig. 2C illustrates that the relative error increases significantly for smaller build plane angle. Struts at 0° show the largest discrepancy from the as-designed thickness, as opposed to vertical struts. An exponential interpolation, $E(\theta, t_d)$, was used in Fig. 2C to estimate the error at each design thickness and generate the compensated strut thickness through the relations:

$$t_c(\theta) = (1 - E(\theta, t_d))t_d \quad \forall \; t_c > 60\ \mu m,$$
$$t_c(\theta) = 60\ \mu m \quad \forall \; t_c \leq 60\ \mu m,$$
$$E(\theta, t_d) = \frac{(t_d - t_m)}{t_d},$$

where $E(\theta, t_d)$ is the relative error from the as-designed strut at a given angle (θ) and strut thickness (t_d), t_c is the compensated strut thickness at a given angle (θ), and t_m is the manufactured strut thickness. A 60 μm threshold was chosen for the compensated thickness to account for the minimum layer thickness of 30 μm. Since the slicing of additive manufactured parts is a form of discretization, the Nyquist sampling theorem was applied as an analog to ensure we can adequately render the structure (Guillemin, 1963). In the mechanical analog, the minimum layer resolution should be at least 30 μm to represent the structure. Hence since a strut is typically discretized with a minimum of 2 sections, the minimum out of plane thickness should be 60 μm.

2.3. Application of the compensation scheme to the spider-web

The compensation scheme was used to obtain the geometry of the compensated spider-web, which was built in five replicates for each strut thickness and with process parameters used for the initial design. Strut thicknesses were measured across all angles (Fig. 2F) with results shown in Fig. 3. In this work, the manufactured strut thickness was defined as the average thickness measured at discrete planes along the strut axis. Here as example, only the set of relative

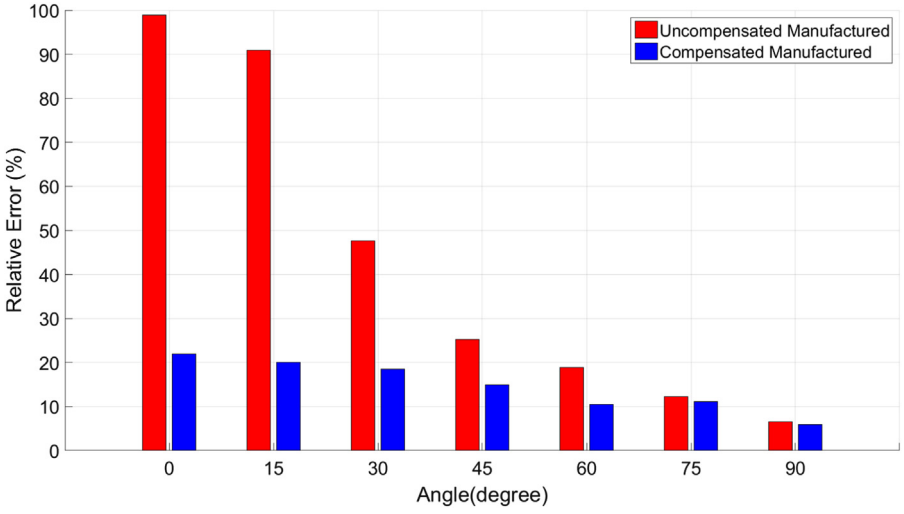

Fig. 3 – Relative error of strut thickness normalized by their as-designed value (200 μm), plotted with respect to the build-plane angle for uncompensated (red) and compensated (blue) spider-webs. (For interpretation of the references to color in this figure legend, the reader is referred to the web version of this article.)

errors for the compensated versus the uncompensated samples is shown for struts with prescribed 200 μm thickness. The most reduced overmelting is observed for the horizontal struts followed by the oblique and vertical struts. In addition, for strut thickness of 200 μm, 300 μm and 400 μm, the average reduction of the relative error is quite consistent and respectively 28%, 20% and 19%.

3. Application of the compensation scheme to metallic lattices for bone replacement

To assess its efficiency in reducing strut thickness discrepancies and improve the fidelity of as-manufactured geometries, the scheme is here applied to three-dimensional porous biomaterials. We select a tetrahedron-based topology, suitable for load-bearing orthopedic implants (Arabnejad et al., 2016a), and use it to generate a representative lattice that meets bone ingrowth requirements, i.e. pore size between 50 and 650 μm and porosity above 50%, and SLM constraints, i.e. manufacturable strut thickness above 200 μm.

3.1. Morphological investigation

3.1.1. Sample geometry

A prismatic porous sample was obtained by tessellating a tetrahedron-based unit cell with x, y and z periodicity of 10, 15 and 10, according to ISO 13314 (ISO 13314, 2011). The sample size consists of 22 mm height and 15.5 mm depth and width. The size of each unit cell is 1.52 mm, the strut thickness is uniform with value of 0.39 mm. A total of 10 samples, 5 uncompensated and 5 compensated, were built via SLM out of Ti–6Al–4V. In addition to the manufacturing process described in Section 2, all samples were annealed at 730 °C for 1 h. Heat treatment results in enhanced mechanical properties while having negligible impact on the morphological parameters (Vrancken et al., 2012a).

3.1.2. Cell morphology assessment

To assess SLM fidelity in rendering cell morphology and overall lattice geometry, a SkyScan 1172 high-resolution micro Computed Tomography (CT), with 103 kV energy and 96 μA intensity, was used on one uncompensated and one compensated sample. During the acquisition process, each sample was rotated by increments of 5° over 360°, and an average of 5 images per increment were recorded as radiograph images. Using dedicated software for micro-CT (NRecon, Skyscab N.V., Kontich, Belgium), the images were processed with lower and upper global thresholds of 80 and 255, ring artifact reduction of 4, and beam-hardening correction of 40%, to enable their reconstruction into cross-section images. These images were in turn used to measure specific morphological parameters, including strut thickness at different angles and pore size, with the ImageJ software package (National Institute of Health, Bethesda, MD) (Rasband, 1997–2015).

3.1.3. Statistical analysis

All data from the morphological characterization were used to perform either a two-tailed *t*-test, when comparing two groups, or a one-way analysis of variances (ANOVA), when comparing more than two groups. The significance level was set at $p<0.05$.

3.1.4. Results

Fig. 4 illustrates the uncompensated (A) and compensated (B) samples, each with a front view of their representative unit cell. The as-designed geometry (hidden red line) is overlaid on the reconstructed images of the uncompensated (C) and compensated (D) unit cell. The former (C) illustrates a larger geometry mismatch. In particular, we highlight i) overmelting of the horizontal struts, ii) stair-case effect of the oblique struts, iii) under-sized vertical struts, as well as iv) parasitic mass agglomerated at the joints. The latter (D) shows the outcome of applying the compensation scheme with each morphological defect reduced in magnitude, and fabricated geometry better resembling the initial design (red).

The as-designed lattice with uniform strut thickness and pore size, was set as a reference to quantitatively address the merit of the compensation strategy with respect to pore size, porosity, and strut thickness. Similarly to other studies (Arabnejad et al., 2016b; Van Bael et al., 2012; Warnke et al., 2009), pore size in this work was defined as the largest sphere that can be inscribed within the cells of a periodic lattice. This definition describes cell interconnectivity in a tetrahedron-based lattice, a property of high biological relevance (Jones et al., 2009; Lin and Miller, 2000). Table 1 summarizes the results with the relative error of the uncompensated (red) and the compensated (blue) manufactured cells reported against the as-designed reference (gray), while Fig. 5 plots their relative error normalized by their as-designed counterparts. The bars show that porosity is less sensitive to manufacturing imperfections, since both compensated and uncompensated lattice have relative error of about 6% ($p=0.03$). Nonetheless for the pore size, the compensation strategy results in a smaller relative error (11% vs. 15%, $p=0.04$) (Fig. 5). As highlighted in Section 2, Fig. 6 shows for the uncompensated samples ($p=0.001$) a significant dependency of strut thickness on of strut angle. For horizontal struts, the maximum relative error is the highest (60%), followed by 18% for oblique struts and 14% for vertical struts. In contrast, compensated lattices have a more uniform distribution of strut thickness, which thus result less sensitive to their orientation with the build plane ($p=0.19$).

3.2. Mechanical analysis

3.2.1. Computation and testing

In this section we investigate the impact of the compensation strategy on the mechanical properties. We compare the mechanics of as-designed and as-manufactured samples via a combination of simulations and experiments.

The reference lattice was modeled and simulated through non-linear finite element analysis (*Abaqus*), to determine its compressive elastic modulus, 0.2% offset strength and first maximum strength (i.e. compressive stress corresponding to the first local maximum in the stress–strain curve (Khanoki and Pasini, 2012)). The base material used for simulations was considered isotropic with 113 GPa Young's modulus, 0.342 Poisson's Ratio and 4430 kg/m^3 density. In addition,

the effective elastic modulus of the uncompensated and compensated samples was obtained via asymptotic homogenization (AH) on a representative volume element (RVE). The objective is to investigate the impact of manufacturing errors on the elastic terms of the effective stiffness matrix (Fig. 7) (Arabnejad and Pasini, 2013).

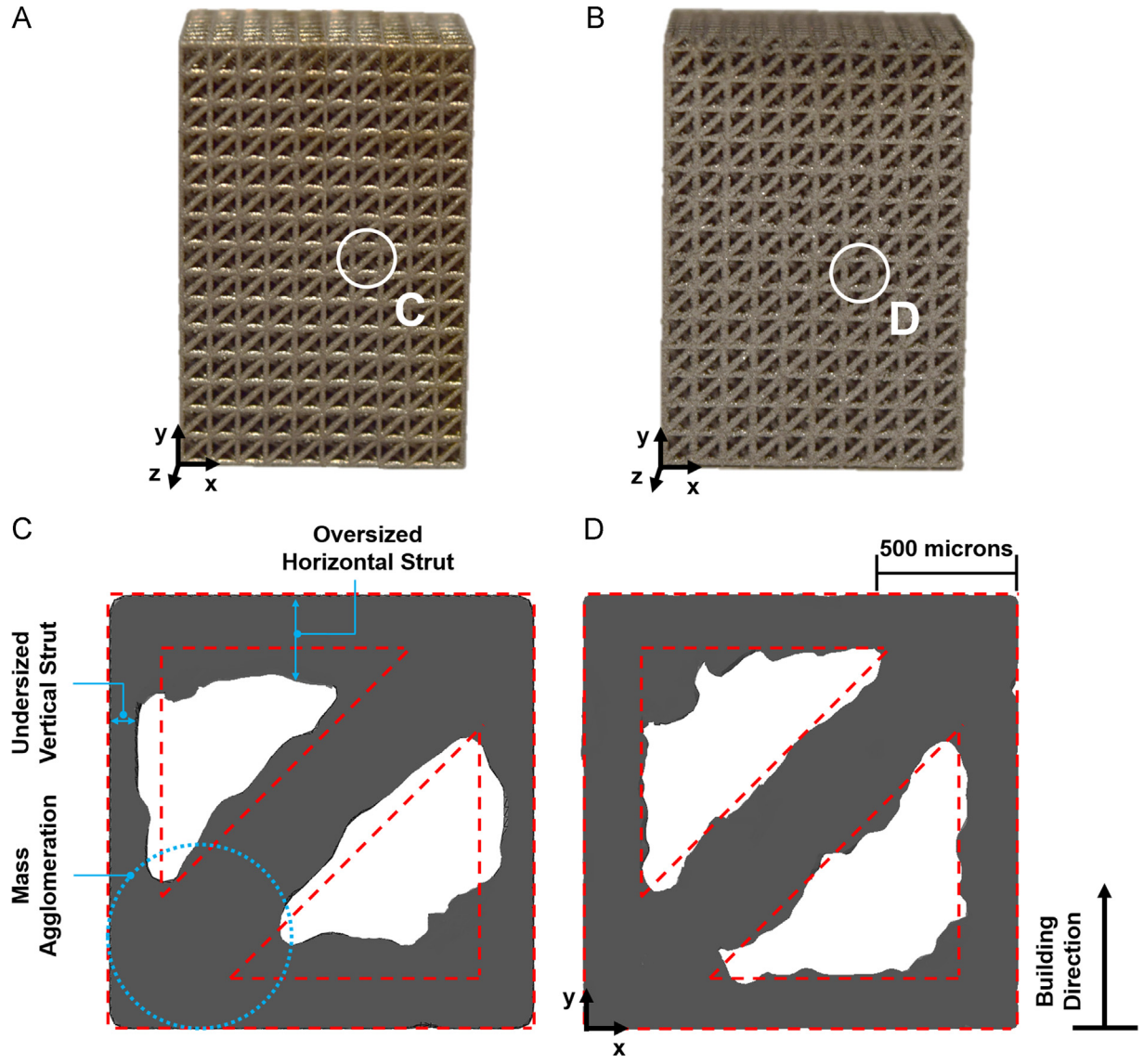

Fig. 4 – Lattice samples and front views of representative reconstructed geometry from micro-CT. A. Uncompensated lattice. B. Compensated lattice. C. Uncompensated representative cell. D. Compensated representative cell. Red hidden lines specify initial design of unit cell. (For interpretation of the references to color in this figure legend, the reader is referred to the web version of this article.)

Table 1 – Morphological variables for as-designed, manufactured uncompensated, and manufactured compensated lattices.

Morphological variables	Pore size [μm]		Porosity [%]		Strut thickness [μm]					
	Value	SD	Value	SD	0		45		90	
					Value	SD	Value	SD	Value	SD
As-designed simulated	500	–	50.0	–	385	–	385	–	385	–
Uncompensated	424	111	53.3	0.3	612	52	317	107	330	43
Error uncompensated	15%	–	6.6%	–	60%	–	18%	–	14%	–
Compensated	445	90	52.7	0.8	397	64	365	72	382	41
Error compensated	11%	–	5.4%	–	3.1%	–	5.3%	–	0.67%	–

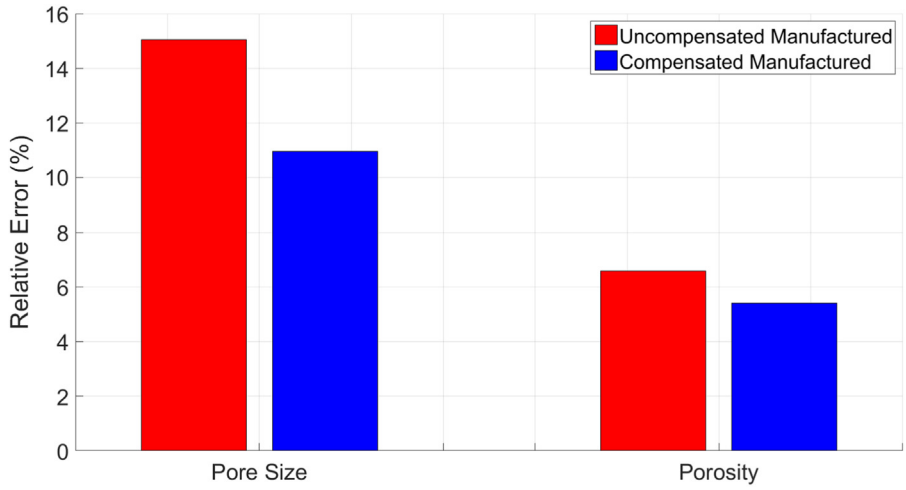

Fig. 5 – Relative error of morphological parameters for uncompensated (red) and compensated (blue) lattices normalized by their as-designed values. (For interpretation of the references to color in this figure legend, the reader is referred to the web version of this article.)

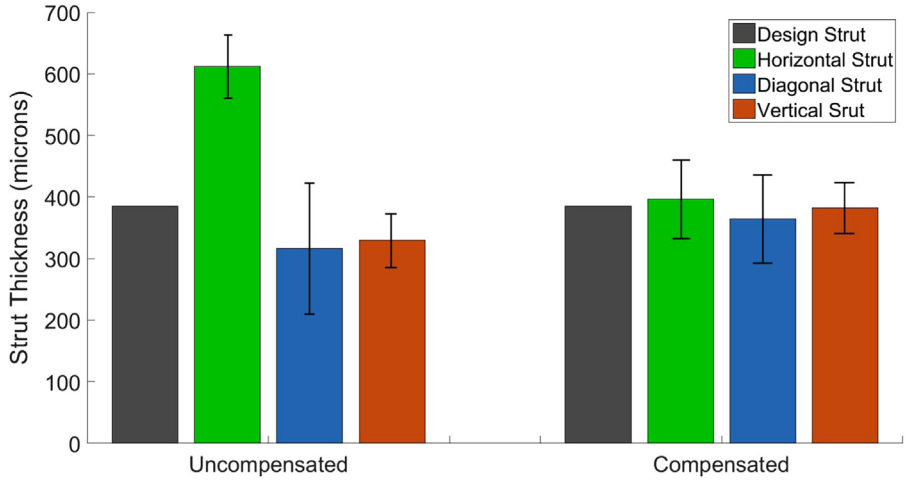

Fig. 6 – Statistical measures of manufactured strut thickness at given strut angle for uncompensated (left) and compensated (right) lattices.

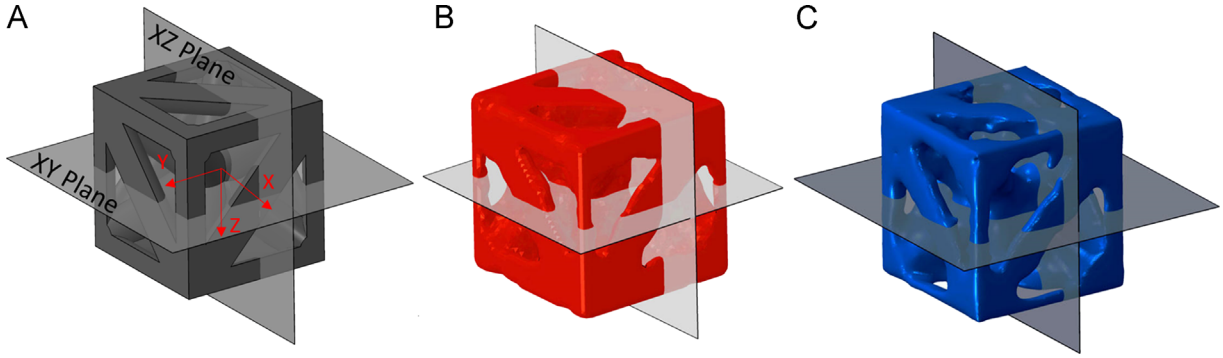

Fig. 7 – Representative tetrahedron-based cell in three scenarios. A. As-designed, B. Uncompensated, i.e. reconstructed from SLM manufactured initial geometry (A). C. Compensated, i.e. reconstructed from SLM manufactured compensated geometry.

All manufactured lattices, five uncompensated and five compensated, were tested in compression in a 50 kN MTS servo-electric machine. As per the ISO-13314 standard, the deformation was measured with an extensometer mounted on the lattice and the elastic modulus was calculated as the slope of the stress–strain curves between 30% and 70% of the plateau strength (ISO 13314, 2011). The yield strength was determined using the 0.2% offset value and the first

maximum strength was obtained directly from the curves. All data from the mechanical testing undergo the statistical analysis described in Section 3.1.

3.2.2. Results

Fig. 8 shows the polar plot of the normalized Young's modulus for the as-designed (Fig. 7A), uncompensated (Fig. 7B) and compensated (Fig. 7C) unit cells. The tetrahedron-based topology has three planes of symmetry, each along a 45° plane not containing the diagonal struts. Both polar plots for the compensated cells (blue) are closer to their as-designed values (black), with those for the uncompensated cells (red) being the most far off; in addition a very minor shift appears in the position of the maximum values for the Young's modulus.

Table 2 reports the as-designed values obtained via a fully detailed finite element analysis of the samples. The compressive elastic modulus is 11.9 GPa, the 0.2% offset strength is 119 MPa, and the first maximum strength is 144 MPa. Fig. 9 illustrates the relative error for the mechanical properties. The relative error of a given property is the difference between the experimental and as-designed value, normalized by the as-designed value and expressed in percentage. The results shows that the compensation strategy reduces significantly the relative error between the as-designed and as-manufactured properties, with errors reduced from 9.50% to 2.74% ($p=0.15$), 31% to 23% ($p=0.02$), and 53% to 22% ($p=0.003$), for respectively compressive elastic modulus, 0.2% offset strength and first maximum strength.

We recall that the current computational results for the designed geometry are obtained considering the material as homogenous regardless the build plane angles. As reported by the AM manufacturer (Renishaw), the building orientation has a negligible impact on the stiffness of SLM titanium parts (horizontal direction=116±1 GPa, vertical direction=112±1 GPa) and 0.2% offset strength (horizontal direction=1045±7 MPa, vertical direction=996±10 MPa) (Innovation, 2015). These results are in agreement with similar reports for titanium alloy components built by SLM and other AM techniques (Simonelli et al., 2014; Vrancken et al., 2012b).

4. Discussion

This study unveils the geometric and mechanical discrepancy between as-designed and as-manufactured geometry of porous biomaterials. Similar observations have been reported in the literature for porous Titanium structures manufactured via commercially available AM processes. Parthasarathy et al. (2010) reported a drop in pore size of the as-manufactured vs. as-designed for porous structures fabricated by Electron Beam Melting. Hollander et al. (2006) noticed a decrease in pore dimension of the as-produced compared to the as-designed structures and a 150 μm mismatch in the strut thickness. Mullen et al. (2010) reported that machine parameters have additional impact on the resulted strut thickness, e.g. increasing laser power results in thicker struts. In Section 2 of this paper,

Table 2 – Mechanical properties of as-designed, uncompensated manufactured, and compensated manufactured porous biomaterials.

Mechanical properties	Stiffness [GPa]		0.2% Offset strength [MPa]		First maximum strength [MPa]	
	Value	SD	Value	SD	Value	SD
As-designed simulated	11.9	–	119	–	144	–
Uncompensated	10.8	0.1	156	6	219	8
Error uncompensated	9.5%	–	31%	–	53%	–
Compensated	12.2	1.7	146	11	175	12
Error compensated	2.7%	–	23%	–	22%	–

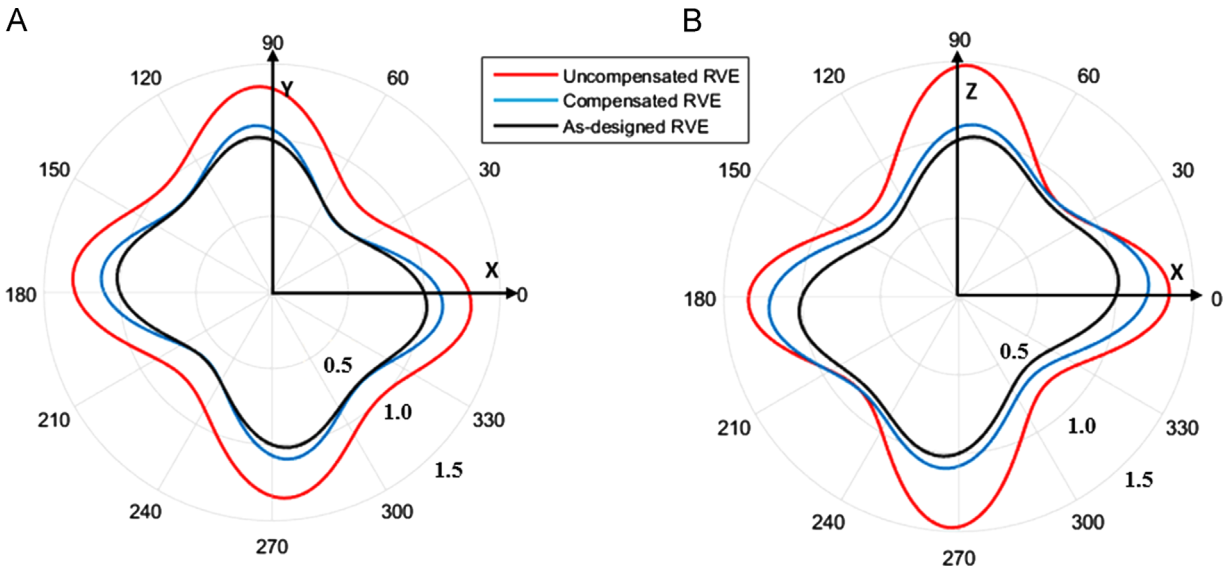

Fig. 8 – Polar plot for the normalized Young's modulus of as-designed, uncompensated and compensated unit cells. A. XY plane. B. XZ plane. Young's moduli normalized with respect to that of the as-designed cell. (For interpretation of the references to color in this figure legend, the reader is referred to the web version of this article.)

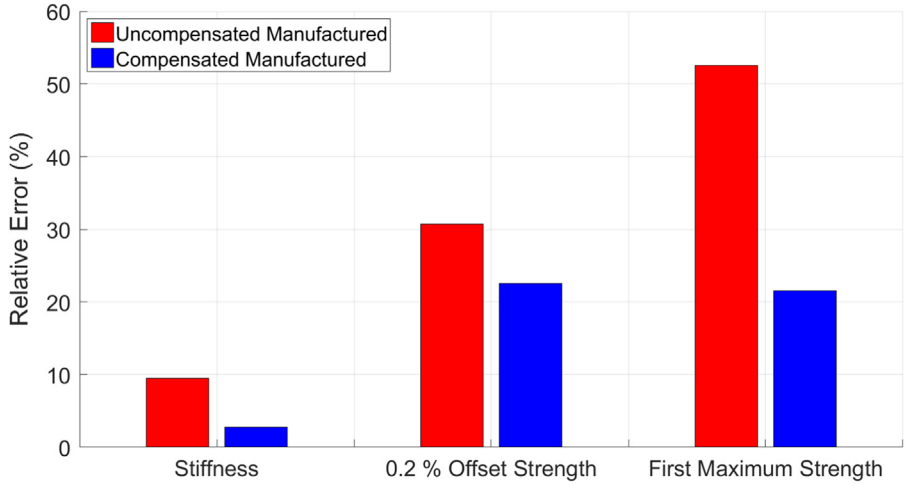

Fig. 9 – Relative error of mechanical properties for uncompensated (red) and compensated (blue) lattices normalized with respect to their as-designed values. (For interpretation of the references to color in this figure legend, the reader is referred to the web version of this article.)

we showed through the spider-web model that strut thickness is highly dependent on the building angle, thereby resulting in over-sized horizontal struts and under-sized vertical struts. We note that these results pertain to cells located at the surfaces of the lattice samples, with measures obtained via two-dimensional light microscopy.

For three-dimensional lattices, Van Bael et al. (2011) reported a significant discrepancy between the as-designed porosity, surface area, and structure volume compared to those of the as-produced lattices. In Section 3 of this paper, we analyzed a three-dimensional lattice structure and confirmed that the manufacturing process yields geometric imperfection in the pore shape and strut thickness. The problem associated with AM can be addressed via either a design oriented or a process-control approach, and this work follows the former. The compensation scheme here proposed has been proved effective in reducing the relative error of the main morphological parameters between the manufactured and designed counterparts with an approximate average drop of 20%. In addition, the application of the scheme enables to render uniform distribution of strut thickness and open pores throughout three-dimensional lattices, thereby showing its merit in producing a porous biomaterials that meet bone ingrowth requirements. Other works focusing on process parameter tuning, such as laser power, scan speed, scan space and powder beat preheat temperature, have been also effective in reducing geometry discrepancy, with dimensional accuracy within 3–8% from the design targets (Eshraghi and Das, 2010; Partee et al., 2005).

The mechanical performance of porous materials is mainly controlled by the cell and sample morphology, described by porosity, pore size, strut thickness and cell size (Williams et al., 2005; Heinl et al., 2008; Hollander et al., 2006; Murr et al., 2009). Thus, geometry mismatch leads to deviations in mechanical properties. We investigated this issue via simulations and experimental measures comparing mechanical properties of compensated and uncompensated lattices. The mismatch of mechanical properties between as-designed and as-manufactured can be attributed to: i) residual stress, caused by dissimilar cooling rate and shrinkage after melting, inducing early strut failure, ii) parasitic particles attached to the strut surface, and iii) local heterogeneities and stress concentration due to strut waviness and strut roughness (Simone and Gibson, 1998a, 1998b).

Previous studies also assessed the discrepancy between the designed and measured mechanical properties for additively manufactured structures. For porous structures, Van Bael et al. (2011) managed to achieve a relative error of 6–15% for the Young's modulus; this was obtained by integrating the mismatch between as-designed and as-produced morphological parameters, using an empirically derived model. Dias et al. (2014) reported that the mechanical properties associated with micro-CT FEA are 18–38% lower than their prescribed values. Likewise, our compensation scheme is efficient in reducing the discrepancies in the elastic (Fig. 8) and plastic (Fig. 9) regimes, and achieve a relative error of 2.7% for the compressive elastic modulus.

Despite the promises of this scheme especially for the elastic properties, there still exists a mismatch of approximately 20% for the 0.2% offset strength and the first maximum strength. The reason can be attributed to the computational results obtained via a fully FEA, here performed on designed geometry, rather than on manufactured geometry. In fact, morphological discrepancies, including material agglomerations at the corners, although reduced, still exist in the compensated samples due to the nature of SLM. A potential strategy to address this issue is to follow a probabilistic method, where the numerical model would include a statistic distributions of the manufacturing defects obtained from the reconstructed geometry. Another solution is to perform FEA on fully reconstructed models obtained via micro-CT images; this choice, however, is very computationally expense and might be unfeasible (Dias et al., 2014).

5. Conclusion

This work has introduced a compensation strategy that can reduce geometric discrepancies appearing in porous biomaterials built via SLM. Developed to capture the dependence of strut thickness on build angle in a spider web, the scheme has been successfully applied to Ti–6Al–4V three-dimensional lattices, with cell topology suitable for load-bearing applications. Results from morphological investigations have proved the merit of the scheme to generate strut thickness, pore-size and porosity closed to their designed values. Mechanical testing and simulations have also confirmed the scheme efficiency in reducing deviations in the mechanical properties of the compensated lattices. This work has used a design-oriented strategy that complements other process-oriented procedures with the goal of further improving SLM accuracy in fabricating porous biomaterials.

Acknowledgments

The authors acknowledge the financial support from the Natural Sciences and Engineering Research Council of Canada (NSERC) and the Canadian Institutes of Health Research (CIHR), as well as the technical support from Mr Mark Kirby and his team from Renishaw Canada.

REFERENCES

Arabnejad, S., Pasini, D., 2013. Mechanical properties of lattice materials via asymptotic homogenization and comparison with alternative homogenization methods. Int. J. Mech. Sci. 77, 249–262 12//.

Arabnejad, S., Burnett Johnston, R., Pura, J.A., Singh, B., Tanzer, M., Pasini, D., 2016a. High-strength porous biomaterials for bone replacement: a strategy to assess the interplay between cell morphology, mechanical properties, bone ingrowth and manufacturing constraints. Acta Biomater. 30, 345–356 Jan 15.

Arabnejad, S., Johnston, R.B., Pura, J.A., Singh, B., Tanzer, M., Pasini, D., 2016b. High-strength porous biomaterials for bone replacement: a strategy to assess the interplay between cell morphology, mechanical properties, bone ingrowth and manufacturing constraints. Acta Biomater. 30, 345–356 Jan.

Arabnejad Khanoki, S., Pasini, D., 2012. Multiscale design and multiobjective optimization of orthopedic hip implants with functionally graded cellular material. J. Biomech. Eng. 134, 031004 Mar.

Arabnejad Khanoki, S., Pasini, D., 2013a. Fatigue design of a mechanically biocompatible lattice for a proof-of-concept femoral stem. J. Mech. Behav. Biomed. Mater. 22, 65–83 6//.

Arabnejad Khanoki, S., Pasini, D., 2013b. The fatigue design of a bone preserving hip implant with functionally graded cellular material. J. Med. Devices 7 020907–020907.

Ashby, M.F., Bréchet, Y.J.M., 2003. Designing hybrid materials. Acta Mater. 51, 5801–5821 11/25/.

Banhart, J., 2001. Manufacture, characterisation and application of cellular metals and metal foams. Prog. Mater. Sci. 46, 559–632 //.

Dias, M.R., Guedes, J.M., Flanagan, C.L., Hollister, S.J., Fernandes, P.R., 2014. Optimization of scaffold design for bone tissue engineering: a computational and experimental study. Med. Eng. Phys. 36, 448–457 Apr.

Eshraghi, S., Das, S., 2010. Mechanical and microstructural properties of polycaprolactone scaffolds with one-dimensional, two-dimensional, and three-dimensional orthogonally oriented porous architectures produced by selective laser sintering. Acta Biomater. 6, 2467–2476 7//.

Fleck, N.A., Deshpande, V.S., Ashby, M.F., 2010. Micro-architectured materials: past, present and future. In: Proceedings of the Royal Society of London A: Mathematical, Physical and Engineering Sciences. Vol. 466, pp. 2495–2516, 2010-09-08 00:00:00.

Gebhardt, A., Hötter, J.-S., Ziebura, D., 2014. Impact of SLM build parameters on the surface quality. RTejournal—Forum Rapid Technol. 5.

Guillemin, E.A., 1963. Theory of Linear Physical Systems: Theory of Physical Systems From the Viewpoint of Classical Dynamics, Including Fourier Methods. Wiley, New York.

Heinl, P., Müller, L., Körner, C., Singer, R.F., Müller, F.A., 2008. Cellular Ti–6Al–4V structures with interconnected macro porosity for bone implants fabricated by selective electron beam melting. Acta Biomater. 4, 1536–1544 2008/09//.

Hollander, D.A., von Walter, M., Wirtz, T., Sellei, R., Schmidt-Rohlfing, B., Paar, O., et al., 2006. Structural, mechanical and in vitro characterization of individually structured Ti–6Al–4V produced by direct laser forming. Biomaterials 27, 955–963 Mar.

Hollister, S.J., Murphy, W.L., 2011. Scaffold translation: barriers between concept and clinic. Tissue Eng. Part B Rev. 17, 459–474 Dec.

Hutmacher, D.W., 2000. Scaffolds in tissue engineering bone and cartilage. Biomaterials 21, 2529–2543.

Innovation R.A., 2015. Ti6Al4V ELI-0406 powder for additive manufacturing, ed.

ISO 13314, 2011. Mechanical testing of metals – Ductility testing – Compression test for porous and cellular metals, International Organization for Standardization, Geneva, Switzerland.

Jones, A.C., Arns, C.H., Hutmacher, D.W., Milthorpe, B.K., Sheppard, A.P., Knackstedt, M.A., 2009. The correlation of pore morphology, interconnectivity and physical properties of 3D ceramic scaffolds with bone ingrowth. Biomaterials 30, 1440–1451 Mar.

Khanoki, S.A., Pasini, D., 2012. Multiscale design and multiobjective optimization of orthopedic hip implants with functionally graded cellular material. J. Biomech. Eng. 134, 10 Mar.

Khoda, A.K.M.B., Ozbolat, I.T., Koc, B., 2010. Engineered tissue scaffolds with variational porous architecture. J. Biomech. Eng. 133 011001–011001.

Lin, C.L., Miller, J.D., 2000. Network analysis of filter cake pore structure by high resolution X-ray microtomography. Chem. Eng. J. 77, 79–86 Apr.

Mullen, L., Stamp, R.C., Fox, P., Jones, E., Ngo, C., Sutcliffe, C.J., 2010. Selective laser melting: a unit cell approach for the manufacture of porous, titanium, bone in-growth constructs, suitable for orthopedic applications. II. Randomized structures. J. Biomed. Mater. Res. B Appl. Biomater. 92, 178–188 Jan.

Murr, L.E., Quinones, S.A., Gaytan, S.M., Lopez, M.I., Rodela, A., Martinez, E.Y., et al., 2009. Microstructure and mechanical behavior of Ti–6Al–4V produced by rapid-layer manufacturing, for biomedical applications. J. Mech. Behav. Biomed. Mater. 2, 20–32 1//.

Murr, L.E., Gaytan, S.M., Medina, F., Lopez, H., Martinez, E., Machado, B.I., et al., 2010. Next-generation biomedical implants using additive manufacturing of complex, cellular and functional mesh arrays. Philosophical Transactions of the Royal Society of London A: Mathematical, Physical and Engineering Sciences. Vol. 368, pp. 1999–2032, 2010-04-28 00:00:00.

Partee, B., Hollister, S.J., Das, S., 2005. Selective laser sintering process optimization for layered manufacturing of CAPA®

6501 Polycaprolactone bone tissue engineering scaffolds. J. Manuf. Sci. Eng. 128, 531–540.
Parthasarathy, J., Starly, B., Raman, S., Christensen, A., 2010. Mechanical evaluation of porous titanium (Ti6Al4V) structures with electron beam melting (EBM). J. Mech. Behav. Biomed. Mater. 3, 249–259 Apr.
Pattanayak, D.K., Fukuda, A., Matsushita, T., Takemoto, M., Fujibayashi, S., Sasaki, K., et al., 2011. Bioactive Ti metal analogous to human cancellous bone: fabrication by selective laser melting and chemical treatments. Acta Biomater. 7, 1398–1406 Mar.
Pyka, G., Burakowski, A., Kerckhofs, G., Moesen, M., Van Bael, S., Schrooten, J., et al., 2012. Surface modification of Ti6Al4V open porous structures produced by additive manufacturing. Adv. Eng. Mater. 14, 363–370.
Rasband, W.S., 1997&;2015. ImageJ. U.S. National Institutes of Health, Bethesda, Maryland, USA.
Ryan, G., Pandit, A., Apatsidis, D.P., 2006. Fabrication methods of porous metals for use in orthopaedic applications. Biomaterials 27, 2651–2670.
Sanz-Herrera, J.A., Kasper, C., Van Griensven, M., Garcia-Aznar, J. M., Ochoa, I., Doblare, M., 2008. Mechanical and flow characterization of Sponceram® carriers: evaluation by homogenization theory and experimental validation. J. Biomed. Mater. Res. - Part B Appl. Biomater. 87, 42–48.
Schaedler, T.A., Jacobsen, A.J., Torrents, A., Sorensen, A.E., Lian, J., Greer, J.R., et al., 2011. Ultralight metallic microlattices. Science 334, 962–965 2011-11-18 00:00:00.
Simone, A.E., Gibson, L.J., 1998a. Effects of solid distribution on the stiffness and strength of metallic foams. Acta Mater. 46, 2139–2150 3/23/.
Simone, A.E., Gibson, L.J., 1998b. The effects of cell face curvature and corrugations on the stiffness and strength of metallic foams. Acta Mater. 46, 3929–3935 7/1/.
Simonelli, M., Tse, Y.Y., Tuck, C., 2014. Effect of the build orientation on the mechanical properties and fracture modes of SLM Ti–6Al–4V. Mater. Sci. Eng.: A 616, 1–11 10/20/.
Sobral, J.M., Caridade, S.G., Sousa, R.A., Mano, J.F., Reis, R.L., 2011. Three-dimensional plotted scaffolds with controlled pore size gradients: effect of scaffold geometry on mechanical performance and cell seeding efficiency. Acta Biomater. 7, 1009–1018 Mar.
Van Bael, S., Kerckhofs, G., Moesen, M., Pyka, G., Schrooten, J., Kruth, J.P., 2011. Micro-CT-based improvement of geometrical and mechanical controllability of selective laser melted Ti6Al4V porous structures. Mater. Sci. Eng.: A 528, 7423–7431 9/15/.
Van Bael, S., Chai, Y.C., Truscello, S., Moesen, M., Kerckhofs, G., Van Oosterwyck, H., et al., 2012. The effect of pore geometry on the in vitro biological behavior of human periosteum-derived cells seeded on selective laser-melted Ti6Al4V bone scaffolds. Acta Biomater. 8, 2824–2834 Jul.
Vrancken, B., Thijs, L., Kruth, J.-P., Van Humbeeck, J., 2012a. Heat treatment of Ti6Al4V produced by selective laser melting: microstructure and mechanical properties. J. Alloy. Compd. 541, 177–185 11/15/.
Vrancken, B., Thijs, L., Kruth, J.P., Van Humbeeck, J., 2012b. Heat treatment of Ti6Al4V produced by selective laser melting: microstructure and mechanical properties. J. Alloy. Compd. 541, 177–185 Nov.
Warnke, P.H., Douglas, T., Wollny, P., Sherry, E., Steiner, M., Galonska, S., et al., 2009. Rapid prototyping: porous titanium alloy scaffolds produced by selective laser melting for bone tissue engineering. Tissue Eng. Part C—Methods 15, 115–124 Jun.
Williams, J.M., Adewunmi, A., Schek, R.M., Flanagan, C.L., Krebsbach, P.H., Feinberg, S.E., et al., 2005. Bone tissue engineering using polycaprolactone scaffolds fabricated via selective laser sintering. Biomaterials 26, 4817–4827.
Wu, S., Liu, X., Yeung, K.W.K., Liu, C., Yang, X., 2014. Biomimetic porous scaffolds for bone tissue engineering. Mater. Sci. Eng.: R: Rep. 80, 1–36 6//.
Yan, C., Hao, L., Hussein, A., Raymont, D., 2012. Evaluations of cellular lattice structures manufactured using selective laser melting. Int. J. Mach. Tools Manuf. 62, 32–38 11//.
Yan, C., Hao, L., Hussein, A., Young, P., Raymont, D., 2014. Advanced lightweight 316 L stainless steel cellular lattice structures fabricated via selective laser melting. Mater. Des. 55, 533–541 3//.
Yang, S., Leong, K.F., Du, Z., Chua, C.K., 2001. The design of scaffolds for use in tissue engineering. Part I. Traditional factors. Tissue Eng. 7, 679–689.